Tidal deformability of neutron stars with realistic nuclear energy density functionals

Young-Min Kim, Yeunhwan Lim, Kyujin Kwak, Chang Ho Hyun, and Chang-Hwan Lee

Phys. Rev. C **98**, 065805 — Published 26 December 2018

DOI: 10.1103/PhysRevC.98.065805

Tidal Deformability of Neutron Stars with Realistic Nuclear Energy Density Functionals

Young-Min Kim,[1] Yeunhwan Lim,[2] Kyujin Kwak,[1] Chang Ho Hyun,[3] and Chang-Hwan Lee[4]

[1]*School of Natural Science, Ulsan National Institute of Science and Technology (UNIST), Ulsan 44919, Korea*

[2]*Cyclotron Institute, Texas A&M University, College Station, TX 77843, USA*

[3]*Department of Physics Education, Daegu University, Gyeongsan 38453, Korea*

[4]*Department of Physics, Pusan National University, Busan 46241, Korea*

(Dated: December 7, 2018)

Abstract

We investigate the constraints on the mass and radius of neutron stars by considering the tidal deformability in the merge of neutron star binaries. We employ models based upon the Skyrme force and density functional theory and select models that are consistent with empirical data of finite nuclei, measured properties of nuclear matter around the saturation density, and observation of the maximum mass of neutron stars. From the selected models, we calculate the Love number k_2, dimensionless tidal deformability Λ, and mass-weighted deformability $\tilde{\Lambda}$ in the binary system. We find that all the models considered in this work give $\tilde{\Lambda}$ less than 800 which is the constraint obtained from the measurement of GW170817. The results from our models show a relationship between Λ and radius ($\Lambda \sim R^{7.5}$) for a neutron star with a fixed mass of $1.4M_{\odot}$, which is consistent with the recent statistical analyses.

I. INTRODUCTION

A series of detections of gravitational wave (GW170817), short γ-ray burst (GRB 170817A), and electromagnetic waves from X-ray to radio bands (AT2017gfo) made it possible to identify the source of the event as the coalescence of two neutron stars [1–3]. From the detection of the phase evolution of gravitational wave during the inspiral phase of merge, one can extract tidal deformability, which characterizes the quadrupole deformation of a neutron star in response to the external quadrupolar gravitational field (i.e., order $l = 2$) [4, 5]. The extent of deformation is closely related to the structure of a neutron star and equation of state (EoS) of matter that consists of the neutron star. Measurement of GW170817 at advanced LIGO and Virgo and its analysis put strong limit on the range of tidal deformability such as $\tilde{\Lambda} \leq 800$ and $\Lambda(1.4M_\odot) \leq 800$ [1] for the case of low-spin priors with 90% confidence level, where $\tilde{\Lambda}$ is combined dimensionless tidal deformability of the binary system and $\Lambda(1.4M_\odot)$ is dimensionless tidal deformability of a single neutron star having a mass of $1.4M_\odot$ [1]. The constraints on $\tilde{\Lambda}$ and $\Lambda(1.4M_\odot)$ obtained from GW170817 exclude stiff EoSs which predict their values larger than 800. In contrast, observations of massive neutron stars with mass $(1.97 \pm 0.04)M_\odot$ [8] and $(2.01 \pm 0.04)M_\odot$ [9] prefer stiff EoSs, ruling out soft EoSs which cannot produce maximum mass larger than these values. Compared with the mass measurement alone, measuring $\tilde{\Lambda}$ has a more advantageous implication that it provides simultaneous constraint on both mass and radius. For example, Ref. [10] performs a model analysis of UV/optical/IR counterpart of GW170817 and obtains a lower bound $\tilde{\Lambda} \geq 400$. However it is shown in Ref. [11] that the models with $\tilde{\Lambda}$ smaller than 400 could still support masses in the interval $(2.1 - 2.3)M_\odot$ which are expected to be compatible with AT2017gfo. With both upper and lower bounds of $\tilde{\Lambda}$, it is now possible to put unprecedented constraint on the EoS of dense nuclear matter.

EoS of nuclear matter is developed and tested in various ways, but data of finite nuclei provide the most essential and fundamental laboratory for them. Depending on the choice of input data and methods of fitting, the number of models that are adjusted to the data

[1] The estimated values are dependent on waveform models and prior assumptions for Bayesian analysis. The dependences and the recent estimations are well described in Ref. [6, 7]. In this work, we use the value of tidal deformability estimated by the initial and minimal-assumption analysis of GW170817 [1], but our results are still consistent with the recent estimation, $\Lambda(1.4M_\odot) = 190^{+390}_{-120}$ at 90% confidence level [7].

of finite nuclei amounts to several hundreds [12]. It has been known that most models are good at producing results consistent with the properties of stable nuclei in the nuclear chart. However, if one moves out of the valley of stability (i.e., moves into the regime of unstable nuclei) and/or calculates EoS at densities away from the saturation density ($\rho_0 = 0.16\,\mathrm{fm}^{-3}$), model predictions do not converge. In this case, models are tested against the properties of nuclear matter which are generally different from those of stable nuclei but can still be measured and/or derived from experiments. A good example can be found in Ref. [12] which calculates the properties of nuclear matter around the saturation density with 240 Skyrme force models and compares them with 11 experimental and/or empirical (i.e, derived from experiments) data (denoted as Exp/Emp). It is found that only 16 models satisfy all 11 Exp/Emp constraints. Additional test for EoS comes from the observation of neutron stars' mass. As mentioned earlier, imposing maximum mass of a neutron star equal to or larger than $2M_\odot$ can rule out models that cannot predict this value of maximum mass. In summary, three sets of constraints, data of stable nuclei, properties of nuclear matter, and the maximum mass of neutron stars, can be used simultaneously for the selection of models in a wide range of density and neutron-proton asymmetry because they provide stringent constraints together.

Recent works on tidal deformability have been focusing on a wide range of EoSs in statistical ways by using a parameterized method (e.g., [11, 13, 14]) or based on the calculation done with about a dozen of representative relativistic mean field models [15]. The conclusions from these works provide a general guideline such that too stiff EoSs are inconsistent with the observation of tidal deformability. What we aim at in the present work is to understand (1) whether non-relativistic models like Skyrme force models give results consistent with preceding works and (2) whether one can have new constraints on the EoS of dense nuclear matter from tidal deformability. For these purposes, it may not be necessary to consider stiff EoSs whose results were already shown in the previous works. More importantly, it is necessary to test EoS based upon both the nuclear physics data and tidal deformability as in this work because as mentioned above, EoS models have been generally tested against the known properties of finite nuclei and nuclear matter before the observation of tidal deformability is available. With this approach, which was not taken in the previous works, we selected our models from the total of 240 Skyrme force models analyzed in Ref. [12].

Our selection is done by applying the aforementioned three constraints and it turns out

that three out of the 240 Skyrme force models have satisfied the three constraints; SkI4 [16], SGI [17], and SLy4 [18]. For comparison, we also include GSkI [19], a model from the generalized Skyrme force models and KIDS [20] from the density functional theory (DFT) models, both of which also satisfy the three constraints.

Note that three selected Skyrme force models are representative Skyrme force models that have been frequently used in many works. For example, our previous works on neutron star with kaons and hyperons, and neutron star cooling showed that these models could provide a framework applicable for the extrapolation to high densities in nuclear matter [21–23]. GSkI is also a well-known extended Skyrme force model and KIDS incorporates a perturbation scheme for the expansion of energy density functional (EDF). Main reason to include these two models is that the structure of the density-dependent interaction terms in GSkI is exactly the same to that in KIDS, so direct comparison of the two models is possible. More details of these models are discussed in a later section. From these models, we obtain the combined dimensionless tidal deformability $\tilde{\Lambda}$ in the range of $360 \leq \tilde{\Lambda}$ $(M_{\rm chirp} = 1.188 M_\odot) \leq 700$. This result is consistent with that from GW170817 and AT2017gfo, $400 \leq \tilde{\Lambda} \leq 800$ [1, 10].

We organize the paper as follows. In Section II, properties and behaviors of selected models are explained. In Section III, we present the results and discuss them in comparison with measurements and predictions from other theoretical works. Section IV concludes our work.

II. MODEL

As mentioned in Sec. I, we consider four representative models, SLy4, SkI4, SGI, and GSkI based upon the Skyrme force model, and a recently developed generalized EDF model, KIDS in this work. We applied three rules to select these models: (i) data of finite nuclei, (ii) properties of nuclear matter near saturation, and (iii) the maximum mass of neutron stars.

Fitting protocol of finite nuclei varies from model to model, so we review and compare them briefly. For the GSkI model fitting data are the binding energies, charge rms radii, single particle energies, and rms radii of valence neutron orbits for 13 spherical nuclei ^{16}O, ^{24}O, ^{40}Ca, ^{48}Ca, ^{48}Ni, ^{56}Ni, ^{68}Ni, ^{78}Ni, ^{88}Sr, ^{90}Zr, ^{100}Sn, ^{132}Sn and ^{208}Pb. In the SLy4 model input data consist of nuclear matter properties, and binding energies, charge radii of doubly closed shell nuclei ^{16}O, ^{40}Ca, ^{48}Ca, ^{56}Ni, ^{78}Ni, ^{100}Sn, ^{132}Sn and ^{208}Pb, and the splitting of

Model	ρ_0	E_0	K_0	$-Q_0$	J	L	$-K_\tau$	$M_{\max}$
Exp/Emp	$\simeq 0.16$	$\simeq 16.0$	$200-260$	$200-1200$	$30-35$	$40-76$	$372-760$	≥ 1.93
CSkP	-	-	$202.0-240.3$	$362.5-425.6$	$30.0-35.5$	$48.6-67.1$	$360.1-407.1$	-
GSkI	0.159	16.02	230.2	405.6	32.0	63.5	364.2	1.98
SLy4	0.160	15.97	229.9	363.1	32.0	45.9	322.8	2.07
SkI4	0.160	15.95	248.0	331.2	29.5	60.4	322.2	2.19
SGI	0.154	15.89	261.8	297.9	28.3	63.9	362.5	2.25
KIDS	0.160	16.00	240.0	372.7	32.8	49.1	375.1	2.14

TABLE I: Properties of nuclear matter and maximum mass of a neutron star calculated with five selected models. Saturation density (ρ_0) is in unit of fm^{-3}. Exp/Emp and CSkP values are quoted from Ref. [12]. E_0, K_0, and Q_0 are binding energy per particle, compression modulus, and skewness (the third derivative of energy per particle) at the saturation density in the symmetric nuclear matter, respectively. J, L, and K_τ are related to the symmetry energy of nuclear matter (see the text for details). E_0, K_0, Q_0, J, L, and K_τ are in unit of MeV and the maximum mass of neutron star ($M_{\max}$) in unit of the solar mass ($M_\odot$).

neutron $3p$ shell in ^{208}Pb. SkI4 model makes use of the binding energies, diffraction radii, surface thickness of ^{16}O, ^{40}Ca, ^{48}Ca, ^{56}Ni, ^{58}Ni, ^{84}Sr, ^{88}Sr, ^{90}Zr, ^{112}Sn, ^{124}Sn, ^{132}Sn, ^{146}Gd, ^{208}Pb, ^{214}Pb, and the spin-orbit splitting between the $1p_{3/2}$ and $1p_{1/2}$ levels in ^{16}O. Compared to these conventional models, KIDS model uses minimal number of data, 17 data from the nuclear matter properties, and 6 data from nuclei, binding energies and charge radii of ^{40}Ca, ^{48}Ca, and ^{208}Pb.

The Skyrme force models have an advantage over the KIDS model that they automatically satisfy well-known properties of finite nuclei since their model parameters are designed to fit them. In contrast, the KIDS model assumes rules to expand nuclear EDF in powers of the Fermi momentum k_F in homogeneous nuclear matter and determines the model parameters in order to reproduce well-known EoS of infinite nuclear matter. After the model parameters are fixed in this way, the model is applied back to calculating the properties of finite nuclei. As a result, in many cases, the properties of finite nuclei calculated with the KIDS model are pure prediction. Therefore, in principle they don't have to be as good as those obtained with

Skyrme force models in reproducing the properties of finite nuclei. However, it is shown that the KIDS model produces a good hierarchical structure in powers of k_F in the homogeneous nuclear matter [20] and reproduces the properties of magic nuclei to an accuracy as good as conventional models [24, 25].

Table I summarizes the properties of nuclear matter at the saturation density and the maximum mass of neutron star calculated from five selected models that have passed our three criteria. Exp/Emp values are also included in the table for comparison. These values were used for the model selection. At the saturation density, the baryon number density of nuclear matter reaches a value of $\rho_0 \approx 0.16$ fm^{-3}. In the symmetric nuclear matter, binding energy (per particle), compression modulus (second derivative of energy per particle), and skewness (third derivative of energy per particle) are denoted as E_0, K_0, and Q_0, respectively, at the saturation density (ρ_0). Nuclear symmetry energy $S(\rho)$, which is caused by the difference in the number of neutron and proton in the nuclear matter, depends on the particle number density (ρ) and is conventionally expanded in powers of $x \equiv (\rho - \rho_0)/3\rho_0$ as

$$S(\rho) = J + L\,x + \frac{1}{2}K_{\rm sym}\,x^2 + \mathcal{O}(x^3)\ , \tag{1}$$

where J, L, and $K_{\rm sym}$ are measured and/or derived from experiments on non-symmetric nuclear matter like (heavy) nuclei having different numbers of protons and neutrons. K_τ in Tab. I is defined as

$$K_\tau \equiv K_{\rm sym} - 6L - \frac{Q_0}{K_0}L\ . \tag{2}$$

Table I shows that the properties of nuclear matter calculated with five selected models are in good agreement with those of Exp/Emp [2].

Considering observational uncertainties in the maximum mass of neutron star, the lowest limit becomes 1.9 $M_\odot$, which we use as a third criterion to select models. Note that five models in Table I can produce the maximum mass above this lowest limit. As indicated in Sec. I, only 16 out of 240 Skyrme force models satisfy all of 11 constraints (denoted by CSkP) based upon the Exp/Emp data of nuclear matter [12]. Eleven constraints are K_0, Q_0, J, L and K_τ at $\rho = \rho_0$, $S(0.5\rho_0)/J$, $P_{\rm PNM}(\rho_0)/L\rho_0$ where $P_{\rm PNM}$ is the pressure in pure

[2] According to Ref. [12], realistic Skyrme force models (denoted by CSkP in Tab. I) predict negative Q_0 values. However a recent analysis with relativistic mean field models shows opposite predictions, positive Q_0 values [26].

neutron matter (PNM), pressure in symmetric nuclear matter (SNM) $P_{\rm SNM}$ in $2\rho_0 < \rho < 3\rho_0$ and $1.2\rho_0 < \rho < 2.2\rho_0$ from two independent data sets, $P_{\rm PNM}$ in $2\rho_0 < \rho < 3\rho_0$, and $E_{\rm PNM}$ in $0.014\rho_0 < \rho < 0.106\rho_0$ where $E_{\rm PNM}$ is the energy per particle in PNM. However, even these 16 *"successful"* models predict a wide range of the maximum mass of neutron star. For instance, the GSkI model satisfies the maximum mass constraint, while the LNS model [27], which belongs to the 16 *"successful"* models, gives the maximum mass less than $1.8M_\odot$. This difference is mainly caused by the fact that the behavior of EoS at high densities varies significantly model to model because it has been known that the maximum mass of neutron star is sensitive to EoS at high densities. We note that among the five models in the current work, GSkI and KIDS satisfy all of 11 constraints of nuclear matter in [12]. (Note that they also satisfy the other two criteria, properties of finite nuclei and the maximum mass of neutron star.) Thus, these two models could be regarded as the most refined model that is consistent with presently available data of finite nuclei, nuclear matter, and neutron star.

It is worth emphasizing again that the maximum mass of neutron star provides a crucial criterion for EoS because it allows us to select specific models whose behavior at the densities much higher than ρ_0 must result in the proper maximum mass of neutron star. As we will see from the results in the following section, tidal deformability can also provide more stringent constraints on both mass and radius of a neutron star.

Phase transition may play an important role in determining the structure of a neutron star and could affect the tidal deformability as well. It can be considered in two major directions, creation of strange hadrons and transition to deconfined quark phase. Hyperons may play an important role in neutron stars because they can reduce the maximum mass of neutron stars by making EoS soft. However, their role is still uncertain; especially, three body effects among hyperons or hyperons and nucleons are quite uncertain. Hence, we decided not to include the results of hyperons in the present work. Concerning the transition to quark matter, it is well known that EoS of quark matter depends heavily on the parameters in the model for deconfined quarks, although existence of quark matter may not satisfy the 2 $M_\odot$ maximum mass constraint unless one uses super-stiff models like NL3. Since the uncertainty in quark phase is also large in dense nuclear matter, we do not consider the topic in the present work, either.

III. RESULT

Tidal deformability (λ) parameterizes the connection between the external quadrupolar tidal field ($\mathcal{E}_{ij}$) and the induced quadrupole moment of a neutron star (Q_{ij}) as

$$Q_{ij} = -\lambda \mathcal{E}_{ij}. \tag{3}$$

Tidal deformability can be represented by the dimensionless tidal Love number k_2,

$$k_2 = \frac{3}{2}\lambda R^{-5}, \tag{4}$$

where R is the radius of a neutron star. In the detection of gravitational waves, the tidal deformability is measured by accumulating the phase differences of gravitational waves. Hence, the dimensionless deformability Λ which naturally appears in the dimensionless phase is commonly used [1, 28, 29];

$$\Lambda = \frac{2}{3}\left(\frac{R}{M}\right)^5 k_2. \tag{5}$$

In a binary system, mass weighted tidal deformability $\tilde{\Lambda}$ is defined with individual deformabilities, Λ_1 and Λ_2, as

$$\tilde{\Lambda} = \frac{16}{13}\frac{(M_1 + 12M_2)M_1^4\Lambda_1 + (M_2 + 12M_1)M_2^4\Lambda_2}{(M_1 + M_2)^5}, \tag{6}$$

where M_1 and M_2 are masses of two neutron stars in the binary [1]. Note that $\tilde{\Lambda} = \Lambda_1 = \Lambda_2$ when $M_1 = M_2$.

Before presenting the results of tidal deformability, we examine the bulk properties of neutron stars predicted from the five selected EoS models in Fig. 1. The upper panel, Fig. 1(a), shows the neutron star mass M as a function of the central density. As expected, all of five models reach the mass $2.0M_\odot$, but the central density (ρ_c) for which the neutron star mass is equal to $2.0M_\odot$ varies from model to model. Similarly, the central density at which the neutron star mass becomes $1.4M_\odot$ also varies among the models. For example, $M = 1.4M_\odot$ when $\rho_c \sim 2.7\rho_0$ for SkI4 and SGI and $\rho_c \sim 3.3\rho_0$ for GSkI, SLy4, and KIDS. The lower panel, Fig. 1(b), plots the predicted mass and radius simultaneously. As in Fig. 1(a), stiff (SkI4 and SGI) and soft (GSkI, SLy4, and KIDS) models behave differently for the mass-radius relation. Note that the three soft models satisfy the constraints of the mass-radius obtained from the Bayesian analyses of X-ray burst observations [30], better than the other two stiff models.

	GSkI	SLy4	SkI4	SGI	KIDS
$R_{1.4M_\odot}$ [km]	11.94	11.82	12.46	12.77	11.79
$k_2(1.4M_\odot)$	0.079	0.077	0.092	0.097	0.076
$\lambda(1.4M_\odot)$ [10^{36}g cm^{2}s^2]	1.906	1.770	2.772	3.292	1.737
$\Lambda(1.4M_\odot)$	337.2	312.9	490.9	583.0	307.5

TABLE II: Radius, tidal Love number, and tidal deformability with and without dimension of a single neutron star with $M = 1.4M_\odot$ calculated from our five EoS models.

The dimensionless tidal deformability (Λ) calculated for a single neutron star is shown as a function of the neutron star mass in Fig. 2. For five models selected in this work, Λ decreases as the neutron star mass increases. As in Fig. 1, our five selected models are divided into two groups, soft (GSkI, SLy4, and KIDS) and stiff (SkI4 and SGI). Note that for $M = 1.4M_\odot$, the soft models predict $\Lambda < 400$ while the stiff models $\Lambda > 400$. However, all the five models satisfy the constraint of the dimensionless tidal deformability ($\Lambda < 800$) at $M = 1.4M_\odot$ which was estimated from GW170817 [1]. For the quantitative comparison with other models, we provide the radius, tidal Love number, and dimensionful and dimensionless tidal deformability calculated for a single neutron star with $1.4M_\odot$ from the five selected models in Table II.

The tidal effect measured in the LIGO/Virgo observations is obtained from the gravitational wave emitted from the merger of two neutron stars. Therefore the quantity most relevant to measurement is the mass-weighted tidal deformability ($\tilde{\Lambda}$) of a binary system. The observations of GW170817 put a constraint on $\tilde{\Lambda}$ such as $\tilde{\Lambda} \leq 800$ for the low-spin prior. With the probable mass ratio $q = 0.7 - 1.0$ which is also estimated from GW170817 for the low-spin prior [1], our selected five EoS models satisfy this constraint of $\tilde{\Lambda}$ in the binary of two neutron stars (see the upper panel of Fig. 3). Note that $\tilde{\Lambda}$ is calculated with Eq. (6) for the merger of two neutron stars with masses M_1 and M_2. Similar to the behaviors of a single neutron star as seen in Fig. 2, the two stiff models (SGI and SkI4) predict larger values of $\tilde{\Lambda}$ than the other three soft models (GSkI, SLy4, and KIDS). Note that the value of $\tilde{\Lambda}$ predicted from the soft models could be less than 400 which is the lower limit estimated in [10]. The mass–weighted tidal deformability ($\tilde{\Lambda}$) can be also drawn as a contour in the Λ_1–Λ_2 space, where Λ_1 and Λ_2 are dimensionless tidal deformability of each neutron star in

the binary. The lower panel of Fig. 3 shows the contour plots obtained from our five models in the Λ_1–Λ_2 space. Note that upper and lower panel of Fig. 3 show the same results in different ways.

Since the first measurement of tidal deformability (Λ and $\tilde{\Lambda}$) from GW170817, several papers have been published already comparing predictions from various models with the measured values. Because it is worth comparing our results obtained from the five selected EoS models with those from previous works, we review some of recent works [13–15, 33] and compare our results with them in the following.

By using tri-tropic and quadru-tropic functions, Ref. [13] constructs more than 20,000 EoSs which are interpolated between the low-density EoS computed with chiral effective field theory [34] and the high-density EoS obtained from non-perturbative QCD [35]. These EoSs are tested against the constraint of $\Lambda(1.4M_\odot) < 800$ and the maximum mass of a neutron star ($M_{\rm max} > 2.0M_\odot$). Radius of a neutron star with $1.4M_\odot$ ($R_{1.4M_\odot}$) is found to be bound between 11.1 km and 13.4 km, consistent with the constraint of the maximum mass and the tidal deformability. If the constraint of $\Lambda(1.4M_\odot)$ were lowered to 400, the radius of the $1.4M_\odot$ neutron star could decrease to 12.3 km. The results obtained for the selected models in our work are in good agreement with those in [13].

In Ref. [15], the EoS models based upon the relativistic mean field (RMF) theory are considered. Ten models are selected first, all of which satisfy the maximum mass of neutron star ($\sim 2M_\odot$), and tested against the tidal deformability. For additional comparison with models they also include measurement of the neutron skin thickness of ^{208}Pb (R_{np}^{208}). This measurement was done by the Lead Radius Experiment (PREX) at the Jefferson Laboratory [36, 37]. Because the radius of a neutron star with $1.4M_\odot$ ($R_{1.4M_\odot}$), tidal deformability ($\Lambda(1.4M_\odot)$ and $\tilde{\Lambda}$), and R_{np}^{208} are predicted together by a given EoS, their correlation can be used to constrain each other. When the constraint of $\Lambda(1.4M_\odot) < 800$ is applied to ten models which predict various radii at a given neutron star mass of $1.4M_\odot$, only four models having relatively soft EoS pass the test. By applying $\Lambda(1.4M_\odot) < 800$ to a radius function fitted to ten models, $R_{1.4M_\odot}$ is estimated less than 13.76 km. Note that this limit on $R_{1.4M_\odot}$ is in good agreement with ours and that in Ref. [13]. The condition $\Lambda(1.4M_\odot) < 800$ also sets an upper limit on the neutron skin thickness as $R_{np}^{208} < (0.25 - 0.28)$ fm, which is obtained with predictions from ten models. However, PREX reports a wide range of measured values, $R_{np}^{208} = 0.33^{+0.16}_{-0.18}$ fm [36, 37]. It is interesting that a substantial portion of PREX value is

ruled out with the constraint of $\Lambda(1.4M_\odot) < 800$. Alternatively, the lower limit of PREX data ($R_{np}^{208} \approx 0.15$ fm) can provide a constraint on the minimum value of $\Lambda(1.4M_\odot)$. Fitted to predictions from ten models, the lower limit on R_{np}^{208} leads to $R_{1.4M_\odot} \approx 12.55$ km and $\Lambda(1.4M_\odot) \approx 490$. If an equal mass binary were assumed, $\tilde{\Lambda} = \Lambda(1.4M_\odot) \approx 490$. This lower limit on $\tilde{\Lambda}$ is larger than 400 which is estimated from AT2017gfo [10]. Note that the lower limit calculated from the models in this work is about 300 as shown in Table II.

Ref. [33] focuses on the role of symmetry energy in EoS. Employing the momentum-dependent interaction (MDI) model, and varying the parameter x in the model which controls stiffness of the EoS such as $x = 0$ (softest limit) to $x = -1$ (stiffest limit), $300 \leq \tilde{\Lambda} \leq 690$ is obtained for an equal mass binary composed of two $1.4M_\odot$ stars. Note that the lower (upper) limit on $\tilde{\Lambda}$ comes from $x = 0$ ($x = -1$). When applied to a single neutron star, the MDI model predicts 11.5 km $\leq R_{1.4M_\odot} \leq$ 13.6 km which also corresponds to between $x = 0$ (lower limit) and $x = -1$ (upper limit). Note that the range of the tidal deformability predicted in [33] is consistent with the results from GW170817 and AT2017gfo, and that the range of $R_{1.4M_\odot}$ is similar to that obtained in [13].

Ref. [14] calculates the tidal deformability with the EoS constrained by chiral effective field theory (EFT) up to twice nuclear saturation density. The effect of uncertainties from high orders and dependence on the momentum cutoff values are analyzed statistically. For the $1.4M_\odot$ mass neutron star, they obtain the radius in the range $10.36 \leq R_{1.4M_\odot} \leq 12.87$ km, and the single star tidal deformability $136 \leq \Lambda(1.4M_\odot) \leq 519$ at the 2σ (95%) confidence level. In Ref. [11] the authors consider a minimal model which is an extrapolation of EoS obtained from EFT up to $2\rho_0$. They obtain $280 \leq \tilde{\Lambda} \leq 480$ for GW170817, which is smaller than another EFT result of [14].

Fig. 4 shows the tidal deformability $\Lambda(1.4M_\odot)$ from the models discussed above. The results from our five selected models are in good agreement with those from the other models [13–15, 33]. In particular, all the data points of the five selected models are on the curve ($\Lambda \sim R^{7.5}$) from [13]. Our results are also consistent with the lower bounds on the deformability and radii of neutron stars estimated using the gravitational waves based on the Bayesian analysis [38].

IV. CONCLUSIONS

The first detection of gravitational wave from the merge of neutron star binary (GW170817) provided valuable information on tidal deformability of merging neutron stars which is determined by the EoS of dense matter inside the neutron star. In order to investigate whether the measured tidal deformability can be predicted with reasonable EoS models which have been tested already against the other sets of criteria, we select five specific EoS models based upon the Skyrme force model and density functional theory. The selected models are SkI4, SGI, SLy4, GSkI, and KIDS and their predictions are in good agreement with three criteria, data of finite nuclei, nuclear matter, and the maximum mass of neutron star. For these five models, dimensionless tidal deformability (Λ) of a single neutron star and mass–weighted tidal deformability ($\tilde{\Lambda}$) of the binary neutron stars are calculated. For a single neutron star with $1.4M_{\odot}$, our five models predict a range of radius 11.8 km $\leq R_{1.4M_{\odot}} \leq$ 12.8 km and a range of dimensionless tidal deformability $308 \leq \Lambda(1.4M_{\odot}) \leq 583$ which satisfies the measured constraint $\Lambda(1.4M_{\odot}) \leq 800$ (see Fig. 2, 4 and Table II). For the mass-weighted tidal deformability ($\tilde{\Lambda}$) of the binary neutron stars, our five models predict $360 \leq \tilde{\Lambda} \leq 700$ for the fixed chirp mass of $M_{\rm chirp} = 1.188M_{\odot}$ and a range of mass ratio $0.7 \leq q = M_2/M_1 \leq 1.0$ which are also estimated from the GW170817 observations for the low-spin prior (see Fig. 3). The predicted range of $\tilde{\Lambda}$ also satisfies the measured constraint $\tilde{\Lambda} \leq 800$, but the lower value of the predicted range is marginal in comparison with the estimated lower limit $\tilde{\Lambda} \geq 400$ from AT2017gfo in [10]. We compare our results with those of recent works and find that our results are in good agreement with them [13–15, 33, 38] while providing a narrower range of predictions due to a smaller number of models in consideration and the absence of phase transition. From our results, however, we can conclude that the first measured tidal deformability from GW170817 is consistent with predictions of models which have been successfully explaining the properties of finite nuclei and nuclear matter as well as the maximum mass of neutron star.

Acknowledgments

YMK and CHL were partially supported by the National Research Foundation of Korea (NRF) grant funded by the Korea government (MSIP and MOE) (No.

2015R1A2A2A01004238, No. 2016R1A5A1013277, and No. 2018R1D1A1B07048599). YL was supported by National Science Foundation under Grant No. PHY1652199. KK was supported by NRF grant by MSIP (No. 2016R1A5A1013277). CHH was supported by the Basic Science Research Program through the NRF funded by the Ministry of Education (NRF-2017R1D1A1B03029020).

---

[1] B. P. Abbott *et al.*, Phys. Rev. Lett. **119**, 161101 (2017).

[2] A. Goldstein *et al.*, Astrophys. J. Lett. **848**, L14 (2017).

[3] B. P. Abbott *et al.*, Astrophys. J. Lett. **848**, L12 (2017).

[4] E. E. Flanagan, and T. Hinderer, Phys. Rev. D **77**, 021502 (2008).

[5] T. Hinderer, Astrophys. J. **677**, 1216 (2008).

[6] B. P. Abbott *et al.*, arXiv:1805.11579v1 [gr-qc] (accepted to Phys. Rev. X).

[7] B. P. Abbott *et al.*, Phys. Rev. Lett. **121**, 161101 (2018).

[8] P. Demorest, T. Pennucci, R. Ransom, M. Roberts, and J. W. T. Hessels, Nature **467**, 1081 (2010).

[9] J. Antoniadis *et al.*, Science **340**, 448 (2013).

[10] D. Radice, A. Perego, F. Zappa, and S. Bernuzzi, Astrophys. J. Lett. **852**, L29 (2018).

[11] I. Tews, J. Margueron, and S. Reddy, Phys. Rev. C **98**, 045804 (2018).

[12] M. Dutra, O. Lourenco, J. S. Sá Martins, and A. Delfino, Phys. Rev. C **85**, 035201 (2012).

[13] E. Annala, T. Gorda, A. Kurkela, and A. Vuorinen, Phys. Rev. Lett. **120**, 172703 (2018).

[14] Y. Lim and J. Holt, Phys. Rev. Lett. **121**, 062701 (2018).

[15] F. J. Fattoyev, J. Piekarewicz, and C. J. Horowitz, Phys. Rev. Lett. **120**, 172702 (2018).

[16] P.-G. Reinhard, and H. Flocard, Nucl. Phys. **A584**, 467 (1995).

[17] Guo-Qiang Li, J. Phys. G **17**, 1 (1991).

[18] E. Chabanat, P. Bonche, P. Haensel, J. Meyer, and R. Shaeffer, Nucle. Phys. **A635**, 231 (1998).

[19] B. K. Agrawal, S. K. Dhiman, and R. Kumar, Phys. Rev. C **73**, 034319 (2006).

[20] P. Papakonstantinou, T.-S. Park, Y. Lim, and C. H. Hyun, Phys. Rev. C **97**, 014312 (2018).

[21] Y. Lim, K. Kwak, C. H. Hyun, and C.-H. Lee, Phys. Rev. C **89**, 055804 (2014)

[22] Y. Lim, C. H. Hyun, K. Kwak, and C.-H. Lee, Int. J. Mod. Phys. E **24**, 1550100 (2015).

[23] Y. Lim, C. H. Hyun, and C.-H. Lee, Int. J. Mod. Phys. E **26**, 1750015-328 (2017).

[24] H. Gil, P. Papakonstantinou, C. H. Hyun, T.-S. Park, and Y. Oh, Acta. Phys. Polon. B **48**, 305 (2017).

[25] H. Gil, P. Papakonstantinou, C. H. Hyun, and Y. Oh, New Physics: Sae Mulli **67**, 456 (2017).

[26] J. Margueron, R. H. Casali, and F. Gulminelli, Phys. Rev. C **97**, 025805 (2018).

[27] L. G. Cao, U. Lombardo, C. W. Shen, and N. V. Giai, Phys. Rev C **73**, 014313 (2006).

[28] T. Hinderer, B. D. Lackey, R. N. Lang, and J. S. Read, Phys. Rev. D **81**, 123016 (2010).

[29] M. Favata, Phys. Rev. Lett. **112**, 101101 (2014).

[30] A. W. Steiner, J. M. Lattimer, and E. F. Brown, Astrophys. J. **722**, 33 (2010).

[31] A. W. Steiner, J. M. Lattimer, and E. F. Brown, Astrophys. J. Lett. **765**, L5 (2013).

[32] A. W. Steiner, C. O. Heinke, S. Bogdanov, C. Li, W. C. G. Ho, A. Bahramian, and S. Han, Mon. Not. Roy. Astron. Soc. **476**, 421 (2018).

[33] P. G. Krastev, and B.-A. Li, arXiv:1801.04620v1 [nucl-th].

[34] I. Tews, T. Krüger, K. Hebeler, and A. Schwenk, Phys. Rev. Lett. **110**, 032504 (2013).

[35] A. Kurkela, P. Romatschke, and A. Vuorinen, Phys. Rev. D **81**, 105021 (2010).

[36] S. Abrahamyan, *et al.*, Phys. Rev. Lett. **108**, 112502 (2012).

[37] C. J. Horowitz *et al.*, Phys. Rev. C **85**, 032501 (2012).

[38] S. De, D. Finstad, J.M. Lattimer, D. A. Brown, E. Berger, and C. M. Biwer, Phys. Rev. Lett. **121**, 091102 (2018).

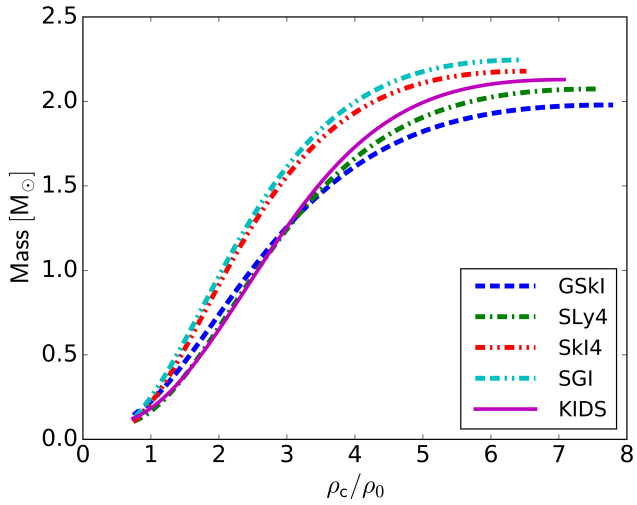

(a) Mass vs. Central Density

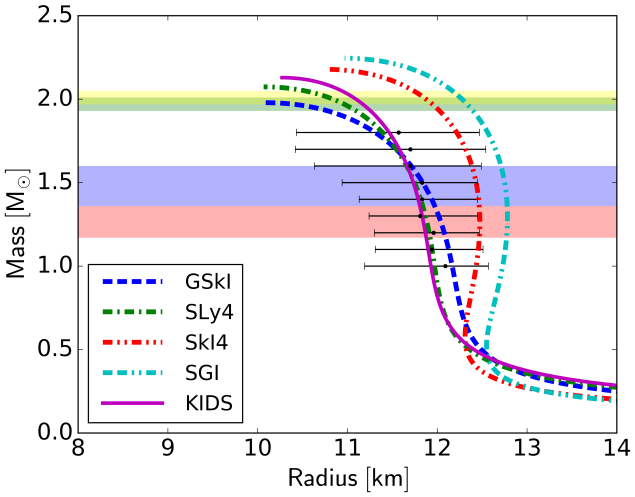

(b) Mass vs. Radius

FIG. 1: Bulk properties of neutron stars predicted from the five selected EoS models described in Sec. II. Top (a) and bottom (b) panels show the neutron star mass as a function of the central density and the mass-radius relationship, respectively. In the bottom panel, yellow and green bands represent the $2M_\odot$ constraint [8, 9], while blue and red bands indicate a neutron star mass of primary (M1) and secondary (M2) in the binary merger, respectively, estimated from GW170817 [1]. Horizontal error bars in the bottom panel (b) indicate the probable (2σ region) radii of neutron stars estimated from the Bayesian analyses of photospheric radius expansion (PRE) X-ray bursts (XRBs) and thermal emission from quiescent low-mass X-ray binaries (qLMXBs) [30]. More recent and updated results on the analyses of PRE XRBs and qLMXBs can be found in Ref. [31, 32]. (Color online)

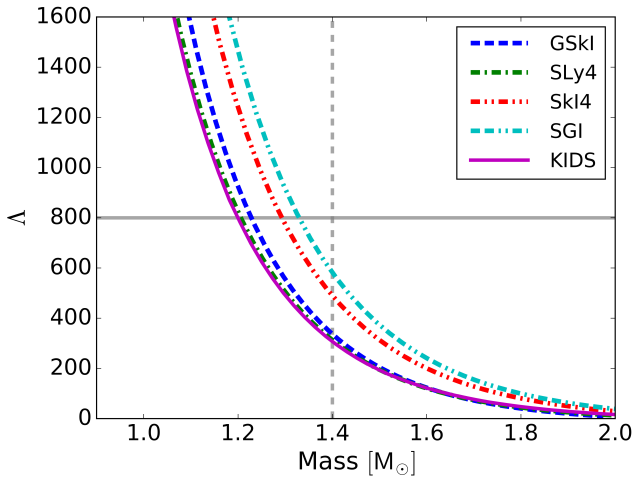

FIG. 2: Dimensionless tidal deformability (Λ) of a single neutron star as a function of mass. A horizontal grey line indicates the constraint of Λ estimated from GW170817 [1]. A vertical grey dotted line corresponds to $1.4M_{\odot}$. (Color online)

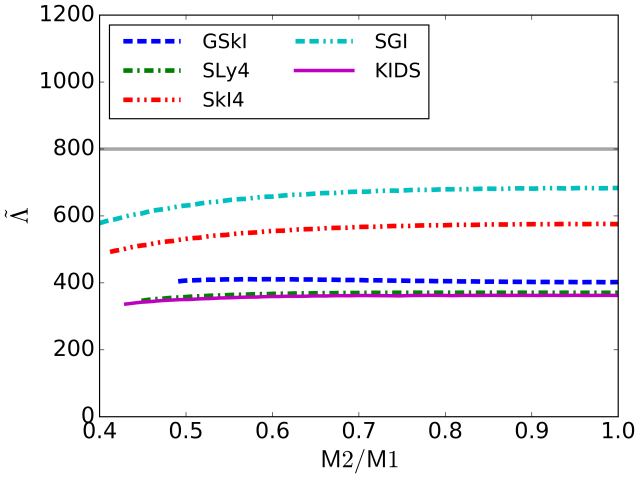

(a) Mass–weighted tidal deformability ($\tilde{\Lambda}$) as a function of mass ratio

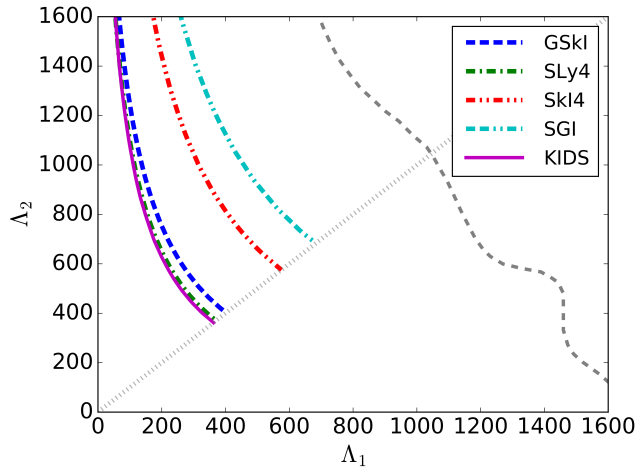

(b) Mass–weighted tidal deformability ($\tilde{\Lambda}$) in the Λ_1–Λ_2 space

FIG. 3: Mass-weighted tidal deformability ($\tilde{\Lambda}$) in the binary of two neutron stars. We fix the chirp mass of the binary at $M_{\rm chirp} = 1.188 M_\odot$ as observed by LIGO/Virgo [1] but allow the mass ratio to vary. The top (a) and bottom (b) panels show $\tilde{\Lambda}$ as a function of mass ratio (M_1/M_2) and in the Λ_1–Λ_2 space, respectively. The horizontal grey line in the top panel is $\tilde{\Lambda} = 800$, the constraint estimated from GW170817. In the bottom panel, a similar constraint is indicated by the grey dashed curve which represents the 90% confidence level of $\tilde{\Lambda} \leq 800$ in the Λ_1–Λ_2 space (i.e., the region below the curve corresponds to $\tilde{\Lambda} \leq 800$ with 90% confidence). The diagonal grey dotted line in the bottom panel corresponds to the case of an equal-mass binary, i.e., $M_1 = M_2 = 1.36 M_\odot$. In this case, $\tilde{\Lambda} = \Lambda_1 = \Lambda_2$. (Color online)

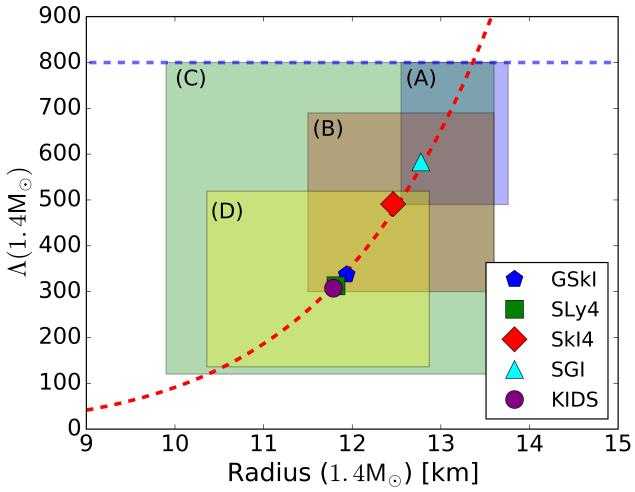

FIG. 4: Dimensionless tidal deformability (Λ) of a single neutron star as a function of radius when the mass of neutron star is fixed at 1.4 $M_{\odot}$. The results from our five models are indicated with color symbols. The shaded rectangles are adopted from the following references: purple (A) [15], brown (B) [33], green (C) [13], and gold (D) [14]. The red dashed curve corresponds to $\Lambda \sim R^{7.5}$ shown in [13] and it overlaps the results from our five models very well. The horizontal blue dashed line ($\Lambda = 800$) indicates again the constraint of Λ estimated from GW170817 [1]. (Color online)